



HAL
open science

New insights on contact angle/roughness dependence on high surface energy materials

Sylvain Giljean, Maxence Bigerelle, Karine Anselme, Hamidou Haidara

► To cite this version:

Sylvain Giljean, Maxence Bigerelle, Karine Anselme, Hamidou Haidara. New insights on contact angle/roughness dependence on high surface energy materials. *Applied Surface Science*, 2011, 257 (22), pp.9631-9638. 10.1016/j.apsusc.2011.06.088 . hal-02584468

HAL Id: hal-02584468

<https://hal.science/hal-02584468>

Submitted on 16 Apr 2024

HAL is a multi-disciplinary open access archive for the deposit and dissemination of scientific research documents, whether they are published or not. The documents may come from teaching and research institutions in France or abroad, or from public or private research centers.

L'archive ouverte pluridisciplinaire **HAL**, est destinée au dépôt et à la diffusion de documents scientifiques de niveau recherche, publiés ou non, émanant des établissements d'enseignement et de recherche français ou étrangers, des laboratoires publics ou privés.

New insights on contact angle/roughness dependence on high surface energy materials

S. Giljean^{a,*}, M. Bigerelle^{b,1}, K. Anselme^c, H. Haidara^c

^a Equipe MMPF – LPMT, EA conventionnée CNRS 4365, IUT Département GMP, Université de Haute-Alsace, 61 rue Albert Camus, 68093 Mulhouse cedex, France

^b Laboratoire Roberval CNRS UMR 6253, Université de Technologie de Compiègne, Centre de Recherches de Royallieu, BP 20529, 60205 Compiègne cedex, France

^c Institut de Science des Matériaux de Mulhouse (IS2M), CNRS LRC7228, Université de Haute-Alsace, 15 rue Jean Starcky, BP 2488, 68057 Mulhouse cedex, France

A B S T R A C T

The relationship between wettability and roughness has been studied on micro-roughened titanium surface after different cleaning procedures. Whereas most studies addressing (super)-hydrophobic behaviors have so far dealt with the wetting of low surface energy and textured substrates in air environment, we here report on a totally novel system and configuration involving the wetting of highly hydrophilic, textured metallic materials in liquid alkane medium, the so-called two liquid phase method. Roughness characterization showed that substrates were isotropic (2D), at a lengthscale much smaller than the size of the drop, with a heterogeneous (vertical) distribution of peaks and valleys. Depending on whether the alkane that initially penetrates and resides in the pores is displaced or not by the water drop (as for air pockets in air environment), we show that different wetting regimes may appear, depending on the cleaning procedure. To our knowledge, this is the first systematic study dealing with the interplay between surface roughness, the wetting behavior and in particular the (super)-hydrophilicity of high surface energy substrates, in non water miscible liquid environments. Whenever competitive processes of liquid/liquid displacement are involved at such high surface energy and textured substrates, such as titanium implant in bone tissue, these results may contribute understanding and predicting their wetting behavior.

Keywords:

Wetting regimes

Roughness

Scale effects

High surface energy materials

Two liquid phase method

1. Introduction

The behavior of a drop was firstly described by Young [1] using a relationship between surface free energy of liquid/fluid (γ_{lf}), solid/liquid (γ_{sl}) and solid/fluid (γ_{sf})

$$\gamma_{sf} - \gamma_{sl} - \gamma_{lf} \cdot \cos \theta_Y = 0 \quad (1)$$

where θ_Y is the Young angle. This relation is formally applicable only on surfaces that are physically smooth and chemically homogeneous. Indeed, it has been shown since that roughness and chemical heterogeneities have a critical influence on contact angle values (CA) [2–10]. This influence of roughness on CA was mainly studied on structured surfaces bearing well ordered micron-to-nanoscale patterns [11–18], with a special focus on “superhydrophilic” and “superhydrophobic” behaviors [19–24]. Numerous authors have

proposed models to describe the relationship between wettability and roughness [25–29]. But most of those models and experiences, dealing in particular with superhydrophobic or superoleophobic properties, mainly involve bulk substrates or outermost surface coatings which are of low surface energy (polymers, wax, and self-assembled molecular films). On those surfaces, a partial to non-wetting behavior is observed with water (in particular), allowing easily modeling and predicting CA values on the corresponding roughened surface textures.

The Wenzel model [29] of wetting on rough surfaces uses the ratio r between the actual surface area supposed to be fully wetted by the liquid, and the projected planar area to describe the relationship between the apparent equilibrium CA measured on the rough surface (θ_W), and the Young angle (θ_Y) of the smooth surface

$$\cos(\theta_W) = r \cdot \cos(\theta_Y) \quad (2)$$

This model, which thus applies only when there is no gas entrapped beneath the drop, was extended by Cassie and Baxter [25] to involve chemical and physical surface heterogeneities, as well as gas entrapment beneath the drop. In that Cassie–Baxter

* Corresponding author. Tel.: +33 03 89 33 75 18; fax: +33 03 89 33 75 05.

E-mail addresses: sylvain.giljean@uha.fr (S. Giljean), maxence.bigerelle@utc.fr (M. Bigerelle), karine.anselme@uha.fr (K. Anselme), hamidou.haidara@uha.fr (H. Haidara).

¹ Current address: Thermique, Ecoulement, Mécanique, Matériaux, Mise en forme, PrOduction (TEMPO) EA 4542, Université de Valenciennes et du Hainaut Cambrésis, Le Mont Houy, 59313 Valenciennes cedex 9, France.

approach, the equilibrium CA θ_{CB} results from each wet surface fraction Φ_i , the intrinsic Young angle on which is θ_{Yi} , according to

$$\cos(\theta_{CB}) = \sum_i \Phi_i \cdot \cos(\theta_{Yi}) \quad (3)$$

The validity of the model of Cassie and Baxter (CB model) was discussed by several authors. From a physical standpoint, Oliver et al. [5] demonstrated that in several cases, CB model does not predict a correct behavior of CA on rough surfaces. At the opposite Wolansky and Marmur [30] demonstrated that CB model was well adapted for sawtooth surfaces. From a chemical viewpoint, Neumann and Good [31] showed that CB model only applies to macroscopic chemical heterogeneities. Considering only physical heterogeneities (roughness), the foundation of the CB and Wenzel models was discussed by Pease [32] and Bartell and Shepard [2,3] who showed that the CA will only depend on the roughness along the triple line, and not on the surface ratios of the heterogeneities beneath the drop. The validity of those models is still under debate [33–41]. Nevertheless, they admitted that CB model using the surface ratios can be applied to homogeneous rough surfaces if the characteristic size of the roughness is small enough against drop size. In our study, the size of the drop compared to the size of the isotropic roughness allows validating both models, and to either consider the triple line or the surface ratio beneath the drop to account for the CA/roughness dependence.

As stated above, the wetting mechanisms on rough (topographically structured) substrates have been essentially discussed and modeled on materials with low surface energy. On the contrary, the wetting behavior of rough substrates of high surface energy materials still remains sparsely investigated and thus misunderstood. Lim et al. [42,43] studied the influence of roughness on CA of titanium surfaces, although this roughness was quantified by the unique R_a value of the arithmetic average of the absolute vertical deviations, ignoring the many other and often more significant roughness parameters. In the biomedical field, a lot of studies have dealt with the understanding of the mechanisms of cell response to roughness of implants [44–47]. Similarly, the wettability of implants is known to be a crucial application parameter and information [48–51]. The wettability of those implants strongly depends on the surface cleaning [52–54] or surface chemical treatment [55]. However, this influence of the cleaning process is not systematically assessed and optimized when measuring CA on these implants in clinical applications, contrary to laboratory experiments where such surface cleaning and assessment (CA, spectroscopy) of samples is common and recurrent. Furthermore, for metal implants that undergo multiple-step treatments and manipulation (roughening, sterilization, packaging), some of which introduce organic contaminations, not only the wettability (CA) is impacted by the surface state and/or cleaning procedure, but also the often desired penetration and anchoring of biological materials into the surface roughness. Most of CA measurements in the biomedical field are made in air environment on metallic implants with different roughness, and using water as the test liquid. These air-contaminated and often *poorly* cleaned metallic surfaces essentially display a low surface energy, as attested by the finite water CAs which are usually measured under those conditions. A particularly interesting exception to that common practice has been proposed by Rupp et al. [56], with the objective to enhance the surface free energy and the hydrophilicity of sandblasted titanium implants. In their approach, these authors developed a procedure in which the implants were produced under N_2 protection and stored in an isotonic NaCl solution to preserve the previously performed chemical surface activation, until implant placement. The *in vivo* results have effectively confirmed their higher osteointegration and a decrease of the healing time in clinical

applications [57,58], highlighting the cleaning and preservation conditions on *in vivo* surface activity of metal implants.

Our objective in this paper was to study the relationship between wettability and roughness on high surface energy metallic implants, presenting a wide range of micro-scale roughness. The roughness was produced by a single full step process that eliminates chemical differences between samples, and generates, at a lengthscale much smaller than the size of the drop, isotropic surface (2D) roughness characterized by a heterogeneous (vertical) distribution of peaks and valleys, at the difference of the patterned surfaces used in most of similar studies [11–16]. Since surface contamination, even at the scale of a monolayer, can drastically modulate the influence of roughness on wetting, especially on high surface energy substrates (metallic implants), the influence of these cleaning effects was systematically assessed and taken into account. As cleaned metallic implants are high surface energy materials, a total spreading is expected and observed in air environment for an efficient surface cleaning procedure and further preservation from contamination. As a consequence, CA measurements were performed using the “two liquid phase” method [59]. In that configuration, spreading of the drop is reduced by the presence of a surrounding non miscible liquid, which creates a lower interface energy γ_{sl^*} at (solid/surrounding liquid) interface, compared to the reference surface energy γ_{sl} in air. A discussion on the structure of the rough interface involving the drop, the metallic substrates and surrounding liquid is finally proposed for the different cleaning methods, to account for the observed CA values and wetting behaviors (regimes). Besides the above practical (biomedical) aspects, we show that under well defined criteria (derivable statistically), the usual and basic roughness parameter R_a can be relevant, in place of the formal surface ratios, for discussing the wetting behavior of an ensemble of rough surfaces which display self-similar topographical features. On such an ensemble of surface textures, our results show that this is the case, provided that the R_a parameters are shown to scale linearly with the essential topographical length-scales of the rough surfaces, and thus with the surface ratios as we show it in the following.

2. Experimental

2.1. Materials and surface preparation

A 5 mm thick plate of pure Titanium grade 1 (ACNIS International) was used in this study. On that Plate 22 areas were electro-eroded using Electrical Discharge Machining on a spark erosion machine (Charmilles S.A) with adjustable parameters (power, electrode diameter) which allow realizing samples covering a wide range of roughness parameters. Then the plate was cut in order to obtain 22 samples of diameter 20 mm, with 22 gradually increasing roughness levels. To illustrate this roughness level, the amplitude roughness parameter R_a ranges from 1.1 μm to 20 μm for roughness level going from 1 to 22. Mirror polished titanium samples with $R_a = 0.01 \mu\text{m}$ were also used as flat reference surface. The polishing has been carried out on a Pedemax 2 automatic polishing machine provided by Struers. Silicon carbide papers from grade 80 to grade 4000 were successively used.

2.2. Sample cleaning

Three different cleaning methods were used in this study in order to evaluate the influence of surface cleaning on the relationship between wettability and roughness. Firstly, a water rinsing followed by nitrogen drying was called “type 0” cleaning. “Type I” cleaning was defined as successive soakings in ultrasonic baths of acetone, cyclohexane and acetone, followed by water rinsing and

nitrogen drying. Finally, “type II” cleaning was defined as “type I” cleaning followed by an argon plasma cleaning processed on a MDS 110 machine (from PLASSYS), at a power of 100 W during 2 min. After cleaning, samples were immediately immersed in octane medium.

2.3. CA measurements

CA was measured by goniometry using G2 system (KRÜSS). As the surface energy was high on metals after plasma cleaning, all CA measurements were performed in the “two liquid phase” configuration by depositing a water drop of 2 μL in octane medium. Octane, provided by Fluka, with 99% purity was used. The water was a twice distilled and deionized water, of surface tension 72.8 mN m^{-1} , as assessed by tensiometry (Wilhelmy plate method). For each sample, at least seven CA values were determined. During the CA measurement, the drops were observed in top view in order to check for their axisymmetry.

2.4. Profilometry

The topography of the electro-eroded samples was recorded by a three dimensional roughness tactile profilometer (TENCOR™ P10). The vertical sensitivity of the profilometer is 10 nm for the z-axis and 50 nm in the plane. Measurements have been achieved using a stylus having a 2 μm tip radius under a 5×10^{-5} N load. Firstly, three dimension (3D) measurements were achieved calculating Abbott curves [60] and usual 3D roughness parameters. The autocorrelation function showed that the roughness could be seen as isotropic justifying a two dimension (2D) roughness treatment. Thus, thirty 2D profiles were randomly recorded on each surface, built with 40,000 points at a 200 $\mu\text{m/s}$ speed with a total length of 8 mm.

2.5. Roughness parameter calculation

In order to quantify the roughness of the samples a methodology already published by our team [61,62] was used. Briefly, profiles were treated in order to mathematically subtract local shape and wave effects using B-spline without including numerical artefacts. The B-spline was calculated using different evaluation lengths from 0.2 μm to the all length of the profile. For small evaluation lengths, shape and wave effects were totally subtracted whereas for high evaluation length only shape effect was subtracted [61,62]. After this mathematical treatment, more than one hundred roughness parameters, including amplitude, frequency, hybrid and fractal parameters were computed on each profile. Considering the drop size, only roughness parameter evaluated at the macroscopic scale are presented in this study.

2.6. Bootstrap treatment

A bootstrap method was used in order to analyse the variations of both roughness and CA measurements. At least 7 CAs were measured on each sample and at least 30 roughness profiles were recorded as described above (Sections 2.3 and 2.4). The bootstrap method consists in drawing and replacing measurements in each population of CA and roughness results. This procedure was reproduced 100 times for each grade. Then the evolution of roughness versus CA after bootstrap was plotted and the eventual correlation between the parameters was calculated.

3. Results

3.1. Roughness characterization

Illustrations of the 3D roughness of electro-eroded samples are shown in Fig. 1 for 4 different roughness levels. This figure

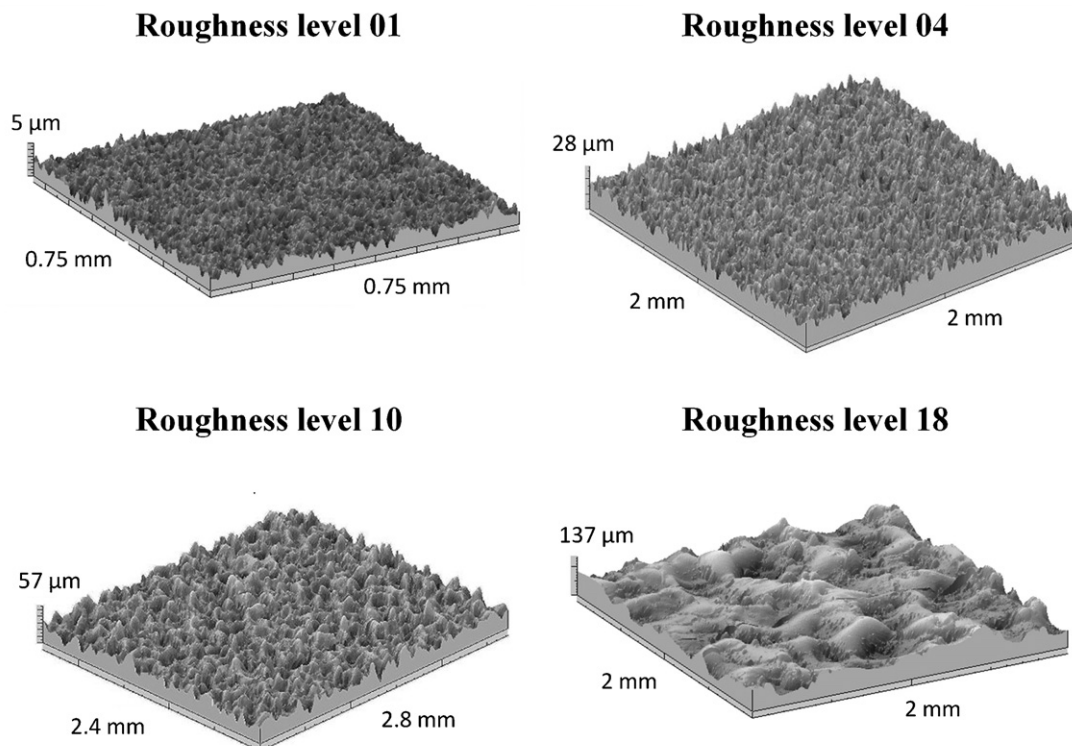


Fig. 1. 3D topography of surfaces obtained by electroerosion process for roughness levels 01, 04, 10 and 18.

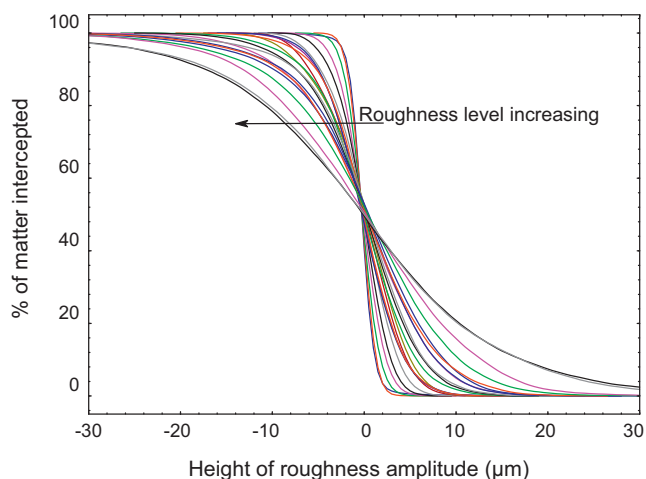


Fig. 2. Abbott curves for the different roughness levels.

represents the morphology obtained by electro-erosion process constituted by adjacent pits, of which diameter depends on experimental parameters such as the diameter of the electrode and the current intensity. As this can be seen in Fig. 1, the electro-erosion process creates an ensemble of surfaces (samples) with roughness features which look self-similar, as higher level “structures” can be seen as a zoom of lower level “structures”. The calculation of the arithmetic roughness R_a and the mean spacing between peaks S_m allowed to find a linear relation between them (supporting material 1). Similar linear relations can be found for every amplitude and frequency roughness parameters. Abbott curves were calculated to give information on height of peaks and depth of valleys (Fig. 2). All curves showed an inflexion point at 50% of matter intercepted, meaning that the topography of peaks and valleys are perfectly symmetric following z-axis. Peak height and valley depth increase concomitantly with roughness level, meaning that an increase of the roughness amplitude involves a proportional increase of the peak-to-valley widths.

3.2. Influence of roughness and cleaning on contact angle values

Top pictures of water drop deposited in an octane medium were recorded before CA measurements. The triple line between octane, water and sample surface kept a circular shape whatever the roughness level (supporting material 2) authorizing the measure of CA. Results of CA measurements versus the arithmetic roughness at the macroscopic scale for the three different cleaning methods are plotted in Fig. 3, after the bootstrap treatment described above (Section 2.6). The roughness parameter R_a was arbitrarily chosen in abscissa since it was shown above (Section 3.1) that the topography was self-similar among the ensemble of the rough samples. As observed in Fig. 3, the cleaning method has a preminent, quantitative and qualitative influence on the relationship between CA and roughness. CAs around 150° were observed with type 0 cleaning and no trivial correlation with the roughness was found. Type I cleaning decreased CA values compared to type 0. For this type I cleaning, a slight increase of CA with increasing roughness was first observed for R_a values ranging from $1.1 \mu\text{m}$ to $2.5 \mu\text{m}$. Then the CA remained constant around 140° in the roughness range between 2.5 and $12 \mu\text{m}$, before it started to decrease for R_a higher than $12 \mu\text{m}$. Finally type II cleaning strongly decreased CA values [63] compared to type 0 and type I cleaning. An increase of CA was observed, when the roughness increased up to a threshold value $R_a = 10 \mu\text{m}$. Above this threshold, CA remained constant at 120° . It thus clearly appears from these results that the more efficient the surface cleaning is,

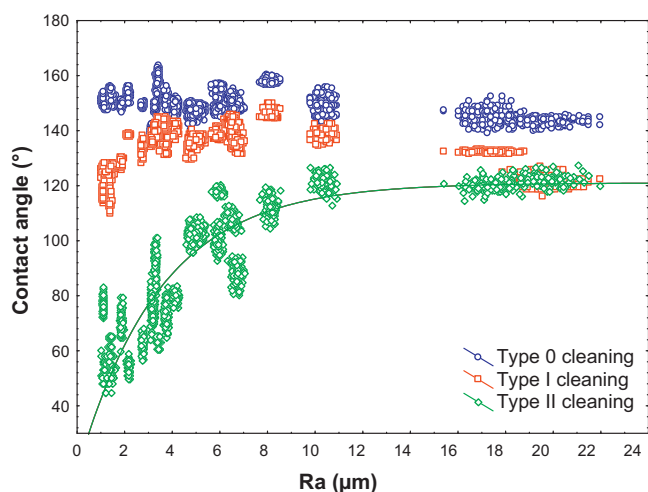


Fig. 3. Evolution of contact angle values versus the roughness for the three different cleaning methods.

the more the correlation between CA and roughness is strong and measurable. To determine the Young equilibrium angle, CAs were measured on mirror polished titanium surfaces in the “two liquid phase” configuration, after the three different cleaning methods. The values obtained for type 0 cleaning, type I cleaning and type II cleaning were respectively $88 \pm 9^\circ$, $85 \pm 3^\circ$ and $16 \pm 6^\circ$. Interestingly, it can be noted here that the Young angle extrapolated from Fig. 3, for the different cleaning are $\sim 150^\circ$, $\sim 110^\circ$ and $\sim 20^\circ$, respectively, for type 0 cleaning, type I cleaning and type II cleaning.

4. Discussion

The two liquid phase configuration can be described as two successive wetting stages on the rough surface (Fig. 4). Firstly the surface is immersed in octane medium. The wetting can either follow the Wenzel or CB model. During the second wetting stage, a water drop is deposited. Wenzel and CB models are again in competition to describe the spreading of the water drop. Finally four wetting configurations, from (a) to (d), have to be considered. The final wetting state depends on the cleaning method.

In order to describe the drop behavior with the different cleaning methods, the spreading parameter S_{SL} defined as:

$$S_{SL} = \gamma_S - \gamma_{SL} - \gamma_L \quad (4)$$

will be used. This parameter characterizes the extent of the wetting of a surface by a liquid, γ_S , γ_{SL} and γ_L being respectively, the surface (interface) free energy of the solid, the solid/liquid and the liquid.

4.1. Type 0 cleaning

With type 0 cleaning, the surface is still covered by usual organic contaminants from ambient air [53], and no significant influence of the roughness on CA values was observed (Fig. 3). On immersion of the substrate in octane the spreading parameter is close to zero, due to both low surface tension of octane and low energy of contaminated surface. One then expects a total spreading in this case, even in the valleys of the rough surface. As a consequence, the octane should totally displace the air, and the wetting can be described by the Wenzel model. During the second wetting stage, two situations can occur. One where a continuous interface between the water drop and the substrate is formed as shown in Fig. 4a, and the second, where a discontinuous interface associating water, octane and substrate is formed (Fig. 4b).

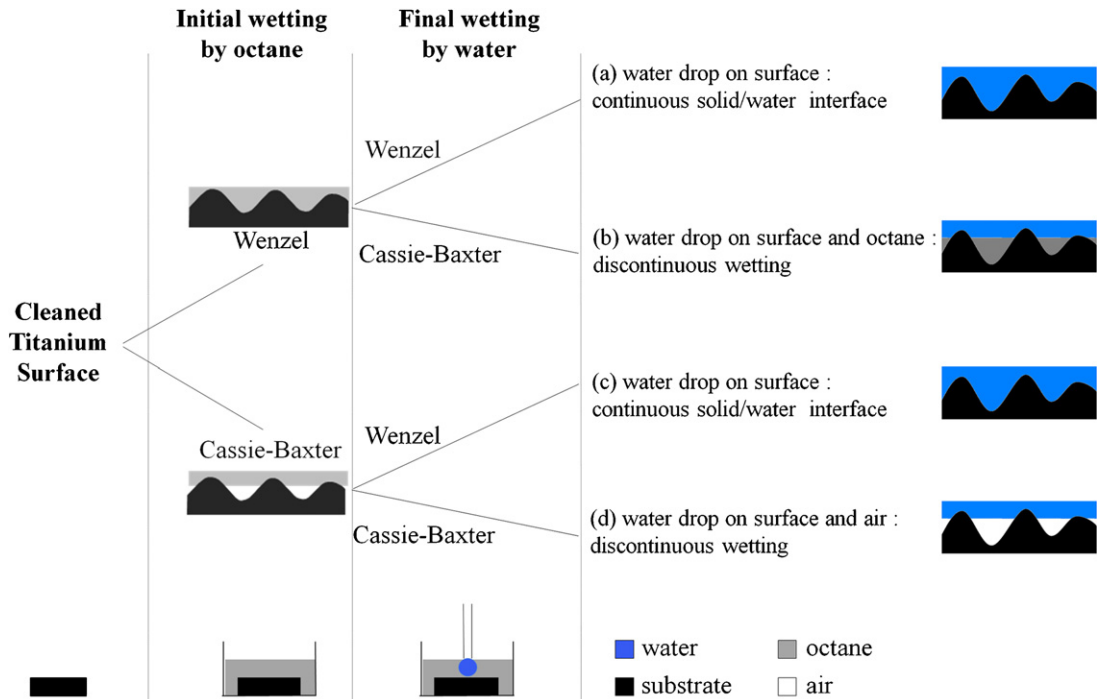


Fig. 4. Different wetting situations on the titanium surface in the two liquid phase configuration using Wenzel or Cassie-Baxter models.

Table 1
"r" ratio defined by Wenzel model at macroscopic scale for the different roughness levels.

| | | | | | | | | | | | |
|----------|-------|-------|-------|-------|-------|-------|-------|-------|-------|-------|-------|
| Level 1 | 2 | 3 | 4 | 5 | 6 | 7 | 8 | 9 | 10 | 11 | |
| r | 1.018 | 1.019 | 1.021 | 1.043 | 1.054 | 1.062 | 1.064 | 1.070 | 1.065 | 1.079 | 1.058 |
| Level 12 | 13 | 14 | 15 | 16 | 17 | 18 | 19 | 20 | 21 | 22 | |
| r | 1.066 | 1.060 | 1.076 | 1.056 | 1.074 | 1.068 | 1.073 | 1.082 | 1.069 | 1.074 | 1.090 |

Both configurations lead to high CA values and explain those measured after type 0 cleaning.

The roughness ratio r of Wenzel, between the actual surface area and the projected planar area, was estimated, at the macroscopic scale (Table 1), to range from 1.02 to 1.09 for the different roughness levels. Using the Young CA value of 88° measured for the water drop on the reference sample in the two liquid-phase configuration, the Wenzel model leads to a CA on the rough surface ranging from 87.82° to 87.95° . It should be noted here that considering the tip radius of the profilometer, the scan size and the sampling frequency, the r values are underestimated [64]. And even if we had higher values of r , the estimated CA by Wenzel model would remain lower than 90° (Eq. (2)). Thus, for r ranging from 1.02 to 1.09, Wenzel model does not predict any change of the CA by surface roughness, and the values of 87.82° and 87.95° are much lower than the measured one of 150° (Fig. 3). As a consequence, the second wetting stage should rather follow the CB model, meaning that some octane remains entrapped beneath the water drop (Fig. 4b). The main point with this type 0 cleaning is that no influence of the roughness is observed on the CA, which remains close to 150° whatever the roughness level. This means that the surface ratios of the octane entrapped beneath the drop are the same whatever the roughness. This ratio can be estimated using CB model [25] which can be rewritten in the following form:

$$\cos(\theta_{CB}) = \Phi_{\text{octane}} \cdot \cos(\theta_{\text{octane}}) + (1 - \Phi_{\text{octane}}) \cdot \cos(\theta_Y) \quad (5)$$

where θ_{CB} is the Cassie-Baxter CA on the rough surface, Φ_{octane} the surface fraction of octane entrapped beneath the drop, θ_{octane} the CA of water on octane, $(1 - \Phi_{\text{octane}})$ the surface fraction of tita-

anium substrate and θ_Y the Young angle on the smooth titanium surface. Since octane and water are non-miscible liquids, the CA between octane and water is formally taken to be 180° . Considering $\theta_{CB} = 150^\circ$, $\theta_Y = 88^\circ$ and $\theta_{\text{octane}} = 180^\circ$ the CA of water on octane, the surface ratio of octane entrapped can be estimated at 87%. With type 0 cleaning, water drop is at rest on the higher picks (Figs. 2 and 4b). With that cleaning, which leaves a material of low surface energy, the two liquid phase configuration would not have been necessary to quantify the CA of the water drop. But this wetting configuration was used for the need to compare the different cleaning methods through same technique.

4.2. Type I cleaning

During the first wetting stage of the cleaned surface (on immersion in octane), the spreading parameter S_{S0} is positive as with type 0 cleaning. The air pockets enclosed in the roughness are totally removed by octane. This means that the first wetting stage follows the Wenzel model as for type 0 cleaning, the rough surface being completely wet by octane. Upon the deposition of the water drop in the second wetting stage, two configurations, from (a) to (b) in Fig. 4, were to be considered. Nevertheless, as shown for type 0 cleaning, the Wenzel model does not predict any change in contact angle value for r ranging from 1.02 to 1.09. The second wetting stage should rather follow the CB model as the CA values depend on roughness value. The surface fraction of octane entrapped beneath the drop, Φ_{octane} , was calculated using the CA value on the reference sample (85°), and those in Fig. 3. The results were plotted in Fig. 5, and values of Φ_{octane} ranging from 50% to about 80% were obtained, with an optimum around $R_a \sim 7 \mu\text{m}$. Far to be an artifact, this apparent optimum may account for the existence of a critical length-scale that determines, together with the surface energies (wetting), the penetration rate of the displacing fluid into the confined rough cavities. Below this length-scale, the penetration is hindered by the geometrical confinement of the cavities (roughness), and increases from zero to an optimum. Above this lengthscale, the geometrical confinement is weaker, and the penetration of the drop is mainly

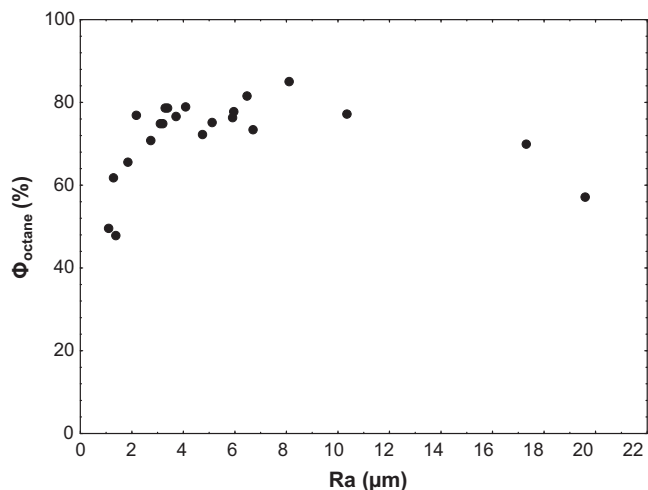


Fig. 5. Surface fraction of octane entrapped beneath the drop (Φ_{octane}) after type I cleaning.

driven by the relative magnitude of the spreading parameter of water (S_{sw}) and octane (S_{so}) on the substrate. Interestingly, it seems in this limit that the penetration rate slightly decreases for this type I cleaning. For each R_a value, Φ_{octane} can be directly converted in terms of peak heights of the rough surface. Indeed, the “fraction (%) of matter intercepted” which is plotted in Fig. 2 corresponds strictly to $(1 - \Phi_{\text{octane}})$ of the CB model. The maximum value of 80% has to be compared with the surface fraction of octane seen by the drop after type 0 cleaning, i.e. 87%. The surface fraction of octane that are entrapped beneath the drop with type 0 and with type I cleaning, must be similarly influenced by the height of the peaks of the rough surface. One then can explain the observed difference of ratio by the fact that the entrapped octane was totally or partially displaced at certain locations by water during the second wetting stage. A part of the cavities is then filled by water, leading to a lower amount of the entrapped phase beneath the drop. This means that a composite wetting model, namely the “hemi-wicking” [40,65] has to be used to describe the wetting configuration of our rough surfaces after type I cleaning. For this cleaning procedure, the “two liquid phase” wetting behavior of the rough, and high surface energy titanium substrate is then well described by the case (b) depicted in Fig. 4.

4.3. Type II cleaning

In the situation of the first wetting of the clean surface by octane, the spreading parameter S_{so} is the highest of the three cleaning methods. As described above for type I cleaning, air enclosed in the roughness is totally removed and the surface is totally wet by octane as described by Wenzel model. In order to study the second wetting, the two spreading parameters, S_{sw} the spreading of water on the solid, and S_{ow} that of water on octane, have to be considered. Considering surface energy values, one has $S_{\text{sw}} \gg S_{\text{ow}}$ since the high surface energy of the cleaned substrate leads here to a very low (surface/water) interface tension. From a thermodynamic point of view, octane should be completely removed by water, leading to case (a) of Fig. 4. Nevertheless the propagation speed of the triple line has to be considered here. The time required to remove octane is higher than the characteristic timescale taken by the triple line for crossing the width of a cavity (valley), essentially due to the high capillary force driving the spreading of the water drop on this high surface energy substrate. Actually, octane can be considered as trapped in the valley by the propagation speed of the triple line. The profile and the displacement of the triple line in this second wetting stage can be described as a succession

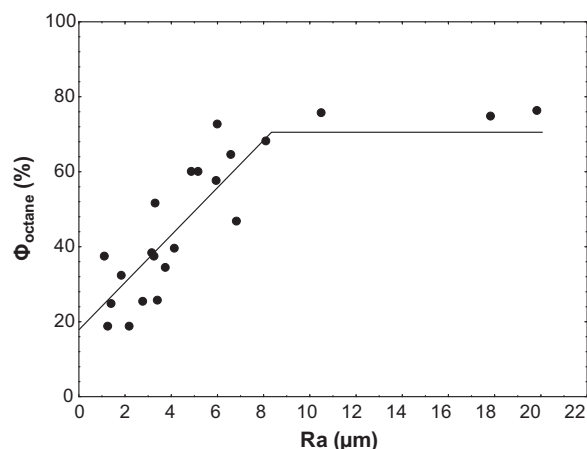


Fig. 6. Surface fraction of octane entrapped beneath the drop (Φ_{octane}) after type II cleaning.

of transient pinning and spreading areas. The protruding titanium surface areas locally pull the triple line ahead, whereas valleys filled by octane act as non-wetted areas, retaining transiently (pinning) the triple line. The final wetting situation consists in a water drop sitting on a mixed surface of titanium and entrapped octane, as described by CB model (Fig. 4b). Using the CA obtained on the reference smooth sample and the results in Fig. 3, the surface fraction of octane entrapped beneath the drop, Φ_{octane} , has been calculated and plotted in Fig. 6. Φ_{octane} linearly increased with the roughness parameter, until a cut off value of roughness above which Φ_{octane} remains constant around 75%. Although involving a different system and wetting configuration, a quite similar result was recently reported by Checco et al. [66] on advancing CA measured in air on a nanostructured surface with cavities. The maximum value of 75% reached here with type II cleaning is the same as that observed with type I cleaning. As described above, this wetting does not follow strictly the Wenzel model, nor that of CB, but a mix of the two with a relative contribution that depends on roughness. Intuitively, for such wetting behavior resulting from the superimposition of both Wenzel and CB models, one would expect two distinct regimes characterized by a jump at the transition, rather than a gradual increase that could be expected for characteristic roughness parameter (size, depth...). The gradual variation of CA observed here may thus account for the non-uniform distribution of the roughness on the substrate. In other words, for a given average roughness parameter R_a , the distribution ranges from $(R_a - \delta)$ to $(R_a + \delta)$. As a result there is always a number of low amplitude (depth) pores ranging in between $(R_a - \delta)$ and R_a , and for which the liquid alkane is displaced from the pores along the contact line. These roughness values of lower amplitude thus determine and contribute for lower CA along the contact line. In the same time, a number of cavities of amplitude (depth) ranging in between R_a and $(R_a + \delta)$ also exists at that average R_a , and for which alkane is no longer displaced from the valleys (cavities). These roughness values of higher amplitude thus determine and contribute for higher CA along the contact line. And as R_a increases, the characteristic amplitude of the “small” cavities is shifted towards larger values, and the total number of pores for which alkane is no longer displaced (even partially) equally increased towards its maximum (for maximum CA). It is therefore the random and isotropic distribution of the roughness around some average value which explains the observed regular variation of CA with the roughness, instead of the theoretically expected jump at some critical roughness R_a^* . This random and isotropic distribution of roughness also contributes to higher standard deviation on contact angle values than usually observed.

It can be noticed that even for the lowest roughness parameter ($R_a = 1.1 \mu\text{m}$) $\Phi_{\text{octane}} = 20\%$. The CA of 16° measured on the reference sample coincides with CA of $\sim 20^\circ$ extrapolated from lowest roughness parameter in Fig. 3. The more the roughness parameter increases, the more the contribution of the Wenzel regime, versus that of CB decreases, until some critical roughness above which the wetting no longer depends on the roughness.

Finally, compared to most of the existing studies in this field, this work constitutes to our knowledge the first systematic investigation of the relationship between CA and roughness, involving a high surface energy material on the one hand, while covering an extended ensemble of roughness textures and parameters which otherwise display a self-similar feature on the other hand. Furthermore, we showed that on such high surface energy materials, the cleaning efficiency has a critical influence on the roughness-dependent wetting regimes (Wenzel, CB, hemi-wicking), contrary to low surface energy materials. With an inefficient cleaning, like the type 0 cleaning, the metallic surface remains hydrophobic with a low surface energy, and the CA/roughness dependence is totally obscured by the residual organic contaminants on the surface. This CA/roughness dependence appears with type I cleaning. Sonication of the samples, in solvents, allows removing metallic or other contaminant particles from the surface [67], but is not sufficient to remove strongly adsorbed surface contamination. Type II cleaning which uses plasma treatment was shown to remove all the surface contamination (mechanically anchored and chemically adsorbed contaminants), leading to partial etching of the native oxide layer under severe experimental conditions [68–70]. With this type II cleaning, the CA/roughness dependence is exalted and readily characterized by the two liquid phase method. The cleaner the surface is, the more the relationship between wettability and roughness can be observed. Furthermore, we showed that for type II cleaning, the activation of the surface energy of the substrate to its maximum, and the high spreading which results from, can lead to a *kinetic entrapment* of the surrounding fluid in the cavities, where surface energy criteria would have dictated the complete displacement of the surrounding fluid.

And finally, regarding the relevance of the usual roughness amplitude parameter R_a , compared to surface ratios of Wenzel and CB relations, it turns out that at identical surface ratios (% of matter intercepted, Fig. 2), it is the peak-to-valley amplitude R_a that critically controls and determines the wetting regimes of rough surfaces. In other words, our results definitely show that the sole surface ratios entering the Wenzel or CB model is totally insufficient for characterizing and accounting for the wetting behavior of rough surfaces.

5. Conclusion

We have used the so-called “two liquid phase method” to investigate the relationship between wetting (contact angles) and roughness on high surface energy titanium materials, for roughness parameter R_a ranging from 1 to 20 μm , and various cleaning procedures of the substrate. We have shown that the observed relation does not only depend on the roughness, but also on the effectiveness of the cleaning procedure. It was shown that the contact angle first increases with the roughness parameter, until a threshold value from which it levels off (plateau). Instead of the jump between distinct wetting regimes, often observed on patterned surfaces for some critical roughness, the increase of the contact angle towards the plateau was here gradual. This was explained by the heterogeneous distribution of the peaks and valleys within the isotropic roughness. The structure of the contact line and wetting mechanism were described by a composite regime (hemi-wicking model) involving the Wenzel and Cassie–Baxter models. The increase of

contact angle with roughness was accounted for an increase of the Cassie–Baxter behavior in the hemi wicking model. Besides its fundamental relevance, this work, involving micro-roughened titanium substrates, is also of particular interest for biomedical applications. Indeed, the competitive displacement of the liquids (water drop and octane here) in the two liquid phase method can constitute a raw model of what goes on between titanium implant and bone tissues, on a rough metallic implant surface.

Alternatively and as a perspective to this work, this investigation may be extended to the captive bubble method. Although the high contact angle (about 180°) of the contacting air bubble and related instability may add further experimental complications, this configuration may reflect more closely the real state of these roughened prostheses materials when exposed (immersed in) a aqueous biological environment.

Acknowledgements

S. Giljean thanks the CNRS and Region Alsace for his PhD thesis funding. This work was also supported by the CETIM (Centre Technique des Industries Mécaniques) foundation, located at Senlis (France) by the Project “Nouvelles méthodes d’analyse des états de surfaces: de la caractérisation à la recherche de paramètres pertinents”.

References

- [1] T. Young, An essay on the cohesion of fluids, Philos. Trans. R. Soc. Lond. 95 (1805) 65–87.
- [2] F.E. Bartell, J.W. Shephard, The effect of surface roughness on apparent contact angles and on contact angle hysteresis. I. The system paraffin–water–air, J. Phys. Chem. 57 (1953) 211–215.
- [3] F.E. Bartell, J.W. Shephard, Surface roughness as related to hysteresis of contact angles. II. The systems paraffin–3 molar calcium chloride solution–air and paraffin–glycerol–air, J. Phys. Chem. 57 (1953) 455–458.
- [4] R.E. Johnson, R.H. Dettre, Contact angle, wettability and adhesion, Adv. Chem. 43 (1964) 112–135.
- [5] J.F. Oliver, C. Huh, S.G. Mason, Apparent contact angle of liquids on finely-grooved solid surfaces – a SEM study, J. Adhes. 8 (1977) 223–234.
- [6] J.F. Oliver, C. Huh, S.G. Mason, Liquid spreading on rough metal surfaces, J. Mater. Sci. 15 (1980) 431–437.
- [7] Y. Tamai, K. Aratani, Experimental study of the relation between contact angle and surface roughness, J. Phys. Chem. 76 (1972) 3267–3271.
- [8] J.F. Oliver, C. Huh, S.G. Mason, An experimental study of some effects of solid surface roughness on wetting, Colloids Surf. 1 (1980) 79–104.
- [9] R.D. Hazlett, On surface roughness effects in wetting phenomena, J. Adhes. Sci. Technol. 6 (1992) 625–633.
- [10] J. Drelich, Y.F. Missirlis, The effect of solid surface heterogeneity and roughness on the contact angle/drop (bubble) size relationship, J. Colloid Interface Sci. 164 (1994) 252–259.
- [11] T.N. Krupenkin, J.A. Taylor, T.M. Schneider, S. Yang, From rolling ball to complete wetting: the dynamic tuning of liquids on nanostructured surfaces, Langmuir 20 (2004) 3824–3827.
- [12] J.T. Yang, Z.H. Yang, C.Y. Chen, D.J. Yao, Conversion of surface energy and manipulation of a single droplet across micropatterned surfaces, Langmuir 24 (2008) 9889–9897.
- [13] T. Sun, G. Wang, H. Liu, L. Feng, L. Jiang, D. Zhu, Control over the wettability of an aligned carbon nanotube film, J. Am. Chem. Soc. 125 (2003) 14996–14997.
- [14] C. Priest, T.W. Albrecht, R. Sedev, J. Ralston, Asymmetric wetting hysteresis on hydrophobic microstructured surfaces, Langmuir 25 (2009) 5655–5660.
- [15] E. Martines, K. Seunarine, H. Morgan, N. Gadegaard, C.D.W. Wilkinson, M.O. Riehle, Air-trapping on biocompatible nanopatterns, Langmuir 22 (2006) 11230–11233.
- [16] W. Choi, A. Tuteja, J.M. Mabry, R.E. Cohen, G.H. McKinley, A modified Cassie–Baxter relationship to explain contact angle hysteresis and anisotropy on non-wetting textured surfaces, J. Colloid Interface Sci. 339 (2009) 208–216.
- [17] J. Bico, U. Thiele, D. Quere, Wetting of textured surfaces, Colloids Surf. A 52 (2006) 157–166.
- [18] A. Marmur, From hydrophilic to superhydrophobic: theoretical conditions for making high contact angle surfaces from low contact angle materials, Langmuir 24 (2008) 7573–7579.

- [19] N. Blondiaux, E. Scolas, A.M. Popa, J. Gavillet, R. Pugin, Fabrication of superhydrophobic surfaces with controlled topography and chemistry, *Appl. Surf. Sci.* 256 (2009) 546–553.
- [20] C.W. Extrand, S.I. Moon, P. Hall, D. Schmidt, Superwetting of structured surfaces, *Langmuir* 23 (2007) 8882–8890.
- [21] E. Martinez, K. Seunarine, H. Morgan, N. Gadegaard, C.D. Wilkinson, M.O. Riehl, Superhydrophobicity and superhydrophilicity of regular nanopatterns, *Nano Lett.* 5 (2005) 2097–2103.
- [22] J. Zhang, Y. Han, A topography/chemical composition gradient polystyrene surface: toward the investigation of the relationship between surface wettability and surface structure and chemical composition, *Langmuir* 24 (2008) 796–801.
- [23] M.R. Cardoso, V. Tribuzi, D.T. Balogh, L. Misoguti, C.R. Mendonça, Laser microstructuring for fabricating superhydrophobic polymeric surfaces, *Appl. Surf. Sci.* 257 (2011) 3281–3284.
- [24] B. Wu, M. Zhou, J. Li, X. Ye, G. Li, L. Cai, Superhydrophobic surfaces fabricated by microstructuring of stainless steel using a femtosecond laser, *Appl. Surf. Sci.* 256 (2009) 61–66.
- [25] A.B. Cassie, S. Baxter, Wettability of porous surfaces, *Trans. Faraday Soc.* 40 (1944) 546–551.
- [26] A.M. Cazabat, M.A. Cohen Stuart, Dynamics of wetting: effects of surface roughness, *J. Phys. Chem.* 90 (1986) 5845–5849.
- [27] P.G. De Gennes, Wetting: statics and dynamics, *Rev. Mod. Phys.* 57 (1985) 827–863.
- [28] R. Shuttleworth, G.L.J. Bailey, The spreading of a liquid over a rough solid, *Disc. Faraday Soc.* 3 (1948) 16.
- [29] R.N. Wenzel, Resistance of solid surfaces to wetting by water, *Ind. Eng. Chem.* 28 (1936) 988–994.
- [30] G. Wolansky, A. Marmur, Apparent contact angles on rough surfaces: the Wenzel equation revisited, *Colloids Surf. A* 156 (1999) 381–388.
- [31] A.W. Neumann, R.J. Good, Thermodynamics of contact angles. I. Heterogeneous solid surfaces, *J. Colloid Interface Sci.* 38 (1972) 341–358.
- [32] D.C. Pease, The contact angle in relation to the solid surface, *J. Phys. Chem.* 49 (1945) 107–110.
- [33] V. Bahadur, S.V. Garimella, Preventing the Cassie–Wenzel transition using surfaces with noncommunicating roughness elements, *Langmuir* 25 (2009) 4815–4820.
- [34] M. Nosonovsky, On the range of applicability of the Wenzel and Cassie equations, *Langmuir* 23 (2007) 9919–9920.
- [35] L. Gao, T.J. Mc Carthy, An attempt to correct the faulty intuition perpetuated by the Wenzel and Cassie “Laws”, *Langmuir* 25 (2009) 7249–7255.
- [36] A. Marmur, E. Bittoun, When Wenzel and Cassie are right: reconciling local and global considerations, *Langmuir* 25 (2009) 1277–1281.
- [37] G. Mc Hale, Cassie and Wenzel: were they really so wrong? *Langmuir* 23 (2007) 8200–8205.
- [38] L. Gao, T.J. Mc Carthy, How Wenzel and Cassie were wrong, *Langmuir* 23 (2007) 3762–3765.
- [39] M.V. Panchagnula, S. Vedantam, Comment on how Wenzel and Cassie were wrong by Gao and McCarthy, *Langmuir* 23 (2007) 13242–13243.
- [40] D.M. Spori, T. Drobek, S. Zurcher, M. Ochsner, C. Sprecher, A. Muhlebach, N.D. Spencer, Beyond the lotus effect: roughness influences on wetting over a wide surface-energy range, *Langmuir* 24 (2008) 5411–5417.
- [41] Y. Kwon, S. Choi, N. Anantharaju, J. Lee, M.V. Panchagnula, N.A. Patankar, Is the Cassie–Baxter formula relevant? *Langmuir* 26 (2010) 17528–17531.
- [42] Y.J. Lim, Y. Oshida, Initial contact angle measurements on variously treated dental/medical titanium materials, *Biomed. Mater. Eng.* 11 (2001) 325–341.
- [43] Y.J. Lim, Y. Oshida, C.J. Andres, M.T. Barco, Surface characterizations of variously treated titanium materials, *Int. J. Oral Maxillofac. Implants* 16 (2001) 333–342.
- [44] K. Anselme, M. Bigerelle, Topography effects of pure titanium substrates on human osteoblast long-term adhesion, *Acta Biomater.* 1 (2005) 211–222.
- [45] J. Lincks, B.D. Boyan, C.R. Blanchard, C.H. Lohmann, Y. Liu, D.L. Cochran, D.D. Dean, Z. Schwartz, Response of MG63 osteoblast-like cells to titanium and titanium alloy is dependent on surface roughness and composition, *Biomaterials* 19 (1998) 2219–2232.
- [46] J.Y. Martin, Z. Schwartz, T.W. Hummert, D.M. Schraub, J. Simpson, J. Lankford Jr., D.D. Dean, D.L. Cochran, B.D. Boyan, Effect of titanium surface roughness on proliferation, differentiation, and protein synthesis of human osteoblast-like cells (MG63), *J. Biomed. Mater. Res.* 29 (1995) 389–401.
- [47] M. Geetha, A.K. Singh, R. Asokamani, A.K. Gogia, Ti based biomaterials, the ultimate choice for orthopaedic implants – a review, *Prog. Mater. Sci.* 54 (2009) 397–425.
- [48] J.I. Rosales-Leal, M.A. Rodriguez-Valverde, G. Mazzaglia, P.J. Ramon-Torregrosa, L. Diaz-Rodriguez, O. Garcia-Martinez, M. Vallecillo-Capilla, C. Ruiz, M.A. Cabrerizo-Vilchez, Effect of roughness, wettability and morphology of engineered titanium surfaces on osteoblast-like cell adhesion, *Colloids Surf. A* 365 (2010) 222–229.
- [49] Y. Arima, H. Iwata, Effect of wettability and surface functional groups on protein adsorption and cell adhesion using well-defined mixed self-assembled monolayers, *Biomaterials* 28 (2007) 3074–3082.
- [50] M. Lampin, R. Warocquier-Clérout, C. Legris, M. Degrange, M.F. Sigot-Luizard, Correlation between substratum roughness and wettability, cell adhesion, and cell migration, *J. Biomed. Mater. Res.* 36 (1997) 99–108.
- [51] J.H. Lee, S.J. Lee, G. Khang, H.B. Lee, The effect of fluid shear stress on endothelial cell adhesiveness to polymer surfaces with wettability gradient, *J. Colloid Interface Sci.* 230 (2000) 84–90.
- [52] R.E. Baier, A.E. Meyer, Implant surface preparation, *Int. J. Oral Maxillofac. Implants* 3 (1988) 9–20.
- [53] B. Kasemo, J. Lausmaa, Biomaterial and implant surfaces: on the role of cleanliness, contamination, and preparation procedures, *J. Biomed. Mater. Res.* 22 (1988) 145–158.
- [54] D.V. Kilpadi, J.E. Lemons, J. Liu, G.N. Raikar, J.J. Weimer, Y. Vohra, Cleaning and heat-treatment effects on unalloyed titanium implant surfaces, *Int. J. Oral Maxillofac. Implants* 15 (2000) 219–230.
- [55] S. Tugulu, K. Löwe, D. Scharnweber, F. Schlottig, Preparation of superhydrophilic microrough titanium implant surfaces by alkali treatment, *J. Mater. Sci. Mater. Med.* 21 (2010) 2751–2763.
- [56] F. Rupp, L. Scheideler, N. Olshanska, M.d. Wild, M. Wieland, J. Geis-Gerstorfer, Enhancing surface free energy and hydrophilicity through chemical modification of microstructured titanium implant surfaces, *J. Biomed. Mater. Res. A* 76A (2006) 323–334.
- [57] D. Buser, N. Broggin, M. Wieland, R.K. Schenk, A.J. Denzer, D.L. Cochran, B. Hoffmann, A. Lussi, S.G. Steinemann, Enhanced bone apposition to a chemically modified SLA titanium surface, *J. Dent. Res.* 83 (2004) 529–533.
- [58] M. Schatzle, R. Mannchen, U. Balbach, C.H. Hammerle, H. Toutenburg, R.E. Jung, Stability change of chemically modified sandblasted/acid-etched titanium palatal implants. A randomized-controlled clinical trial, *Clin. Oral. Implants Res.* 20 (2009) 489–495.
- [59] J. Schultz, M. Nardin, Determination of the surface energy of solids by the two liquid phase method, in: M.E. Schrader, G. Loeb (Eds.), *Modern Approaches to Wettability: Theory and Applications*, Plenum Press, New York, 1992, pp. 73–99.
- [60] E.J. Abbott, F.A. Firestone, Specifying surface quality, *Mech. Eng.* 59 (1933) 569–572.
- [61] S. Giljean, M. Bigerelle, K. Anselme, A multiscale topography analysis of grinded stainless steel and titanium alloys, *Proc. IMechE Part B: J. Eng. Manuf.* 221 (2007) 1407–1420.
- [62] S. Giljean, D. Najjar, M. Bigerelle, A. Iost, Multiscale analysis of abrasion damage on stainless steel, *Surf. Eng.* 24 (2008) 8–17.
- [63] M.C. Kim, D.K. Song, H.S. Shin, S.-H. Baeg, G.S. Kim, J.-H. Boo, J.G. Han, S.H. Yang, Surface modification for hydrophilic property of stainless steel treated by atmospheric-pressure plasma jet, *Surf. Coat. Technol.* 171 (2002) 312–316.
- [64] P.J. Ramon-Torregrosa, M.A. Rodriguez-Valverde, A. Amirfazli, M.A. Cabrerizo-Vilchez, Factors affecting the measurement of roughness factor of surfaces and its implications for wetting studies, *Colloids Surf. A: Physicochem. Eng. Aspects* 323 (2008) 83–93.
- [65] D. Quere, Rough ideas on wetting, *Physica A* 313 (2002) 32–46.
- [66] A. Checco, T. Hofmann, E. DiMasi, C.T. Black, B.M. Ocko, Morphology of air nanobubbles trapped at hydrophobic nanopatterned surfaces, *Nano Lett.* 10 (2010) 1354–1358.
- [67] M.T. Filho, M.R. Leonardo, K.C. Bonifacio, F.R. Dametto, A.B. Silva, The use of ultrasound for cleaning the surface of stainless steel and nickel–titanium endodontic instruments, *Int. Endod. J.* 34 (2001) 581–585.
- [68] B.O. Aronsson, J. Lausmaa, B. Kasemo, Glow discharge plasma treatment for surface cleaning and modification of metallic biomaterials, *J. Biomed. Mater. Res.* 35 (1997) 49–73.
- [69] K.M. Swart, J.C. Keller, J.P. Wightman, R.A. Draughn, C.M. Stanford, C.M. Michaels, Short-term plasma-cleaning treatments enhance in vitro osteoblast attachment to titanium, *J. Oral. Implantol.* 18 (1992) 130–137.
- [70] C. Tendero, C. Tixiera, P. Tristanta, J. Desmaison, P. Leprince, Atmospheric pressure plasmas, a review, *Spectrochim. Acta Part B* 61 (2006) 2–30.